Cell

# Selective Bypass of a Lagging Strand Roadblock by the Eukaryotic Replicative DNA Helicase

Yu V. Fu,[1] Hasan Yardimci,[1] David T. Long,[1,7] The Vinh Ho[2,4,7] Angelo Guainazzi,[2,5,7] Vladimir P. Bermudez,[3] Jerard Hurwitz,[3] Antoine van Oijen,[1,6] Orlando D. Schärer,[2] and Johannes C. Walter[1,*]
[1]Department of Biological Chemistry and Molecular Pharmacology, Harvard Medical School, Boston, MA 02115, USA
[2]Department of Pharmacological Sciences and Chemistry, Stony Brook University, Stony Brook, NY 11794, USA
[3]Program of Molecular Biology, Memorial Sloan Kettering Cancer Center, 1275 York Avenue, New York, NY 10021
[4]Present address: Tecan Group Ltd., 8708 Männedorf, Switzerland
[5]Present address: Helsinn Therapeutics (U.S.) Inc., Bridgewater, NJ 08807, USA
[6]Present address: The Zernike Institute for Advanced Materials, University of Groningen, 9747 AG Groningen, The Netherlands
[7]These authors contributed equally to this work
*Correspondence: johannes_walter@hms.harvard.edu
DOI 10.1016/j.cell.2011.07.045

## SUMMARY

The eukaryotic replicative DNA helicase, CMG, unwinds DNA by an unknown mechanism. In some models, CMG encircles and translocates along one strand of DNA while excluding the other strand. In others, CMG encircles and translocates along duplex DNA. To distinguish between these models, replisomes were confronted with strand-specific DNA roadblocks in *Xenopus* egg extracts. An ssDNA translocase should stall at an obstruction on the translocation strand but not the excluded strand, whereas a dsDNA translocase should stall at obstructions on either strand. We found that replisomes bypass large roadblocks on the lagging strand template much more readily than on the leading strand template. Our results indicate that CMG is a 3′ to 5′ ssDNA translocase, consistent with unwinding via "steric exclusion." Given that MCM2-7 encircles dsDNA in G1, the data imply that formation of CMG in S phase involves remodeling of MCM2-7 from a dsDNA to a ssDNA binding mode.

## INTRODUCTION

In eukaryotic cells, DNA replication initiates at many chromosomal locations called origins. At each origin, two "sister" replisomes are assembled that move away from the origin in opposite directions. An essential component of the replisome is the replicative DNA helicase, which unwinds parental DNA, generating substrates for leading and lagging strand DNA polymerases. Current evidence indicates that the eukaryotic replicative DNA helicase contains at least three components, a heterohexameric ATPase called MCM2-7 and two cofactors, Cdc45 and GINS (Bochman and Schwacha, 2009; Ilves et al., 2010; Moyer et al., 2006; Pacek et al., 2006; Takahashi et al., 2005). The complex of Cdc45, MCM2-7, and GINS is called CMG (Moyer et al., 2006).

A striking feature of eukaryotic DNA replication is the intricate, bi-phasic assembly of CMG, which underlies the cell cycle regulation of DNA replication (reviewed in Arias and Walter, 2007; Labib, 2010). CMG assembly is best understood in yeast. In the G1 phase, when cyclin-dependent kinase (CDK) activity is low, ORC, Cdc6, and Cdt1 recruit MCM2-7 onto origins of DNA replication, forming a prereplication complex (pre-RC). Within the pre-RC, MCM2-7 complexes bind to double-stranded DNA (dsDNA) as inactive double hexamers (Evrin et al., 2009; Gambus et al., 2011; Remus et al., 2009) At the G1/S transition, when CDK activity rises, numerous additional factors cooperate to convert the MCM2-7 double hexamer into two CMG complexes. In particular, Cdc7-Dbf4 protein kinase (DDK) phosphorylates MCM2-7 (Randell et al., 2010 and references therein). CDK phosphorylates Sld2 and Sld3 (Treslin/Ticrr in metazoans), promoting their interaction with Dpb11 (TopBP1 in metazoans). The Sld3-Sld2-Dpb11 complex enables the stable binding of Cdc45 and GINS to phosphorylated MCM2-7. Once formed, CMG unwinds the origin, allowing replisome assembly. Importantly, the high CDK activity present in the S and G2 phases inhibits the functions of ORC, Cdc6, and Cdt1, such that de novo MCM2-7 recruitment is blocked. As a result, CMG complexes that leave the origin during the first initiation event cannot be replaced, and each origin fires only once. Although the regulation of CMG assembly in metazoans is very similar, it appears to be even more complicated, depending on several additional factors, including Mcm9, DUE-B, GEMC1, Geminin, and $CRL4^{Cdt2}$.

A crucial question in the field is why so many proteins are required to convert bound MCM2-7 complexes into the active CMG helicase. This question is inextricably connected to another open question, which is how CMG unwinds DNA in S phase. Only by describing the final disposition of CMG on DNA will it be possible to understand how it is assembled and activated. MCM2-7, the core molecular motor of CMG, is composed of six related AAA+ ATPase subunits, Mcm2-Mcm7 (Tye, 1999).

Thus, GINS and Cdc45 have been proposed to bind to the outside of the MCM2-7 complex and to regulate its ATPase activity (Ilves et al., 2010). Crystallography and electron microscopy reveal that eukaryotic and archaeal MCM complexes form ring-shaped hexamers whose central channel can accommodate single-stranded DNA (ssDNA) or dsDNA (Evrin et al., 2009; Fletcher et al., 2003; Pape et al., 2003; Remus et al., 2009). Thus, DNA unwinding likely involves one or both strands of the DNA passing through the MCM central channel.

Most well-studied replicative DNA helicases, such as *E. coli* DnaB and Bacteriophage T7 gene product 4 (T7 gp4), function as single hexamers that encircle and translocate along one strand of DNA while excluding the other strand ("steric exclusion"). In biochemical experiments using purified proteins, archaeal and eukaryotic MCM proteins including the CMG translocated along ssDNA in the 3′ to 5′ direction (Bochman and Schwacha, 2008; Ilves et al., 2010; Kelman et al., 1999; Moyer et al., 2006; Shechter et al., 2000). Using elegant manipulation of DNA templates, steric exclusion by a purified Mcm4/6/7 subcomplex was directly demonstrated (Kaplan et al., 2003). However, the physiological relevance of these studies is not clear since the reactions bypassed the endogenous helicase loading and activation pathway.

More recently, several considerations led to speculation that CMG might unwind DNA by translocating along dsDNA (Laskey and Madine, 2003; Mendez and Stillman, 2003; Takahashi et al., 2005). First, Mcm4/6/7 can translocate along dsDNA with considerable force (Kaplan et al., 2003). Second, MCM2-7 interacts with dsDNA as part of the pre-RC (Evrin et al., 2009; Remus et al., 2009). It is therefore attractive to propose that MCM2-7 does not fundamentally change its interaction with DNA upon assembly into the CMG. Several models propose how CMG might unwind DNA while translocating along dsDNA. One idea is that CMG functions as an obligate dimer that pumps dsDNA toward its dimer interface, and that single-stranded DNA is extruded through lateral channels, analogous to a mechanism proposed for SV40 large T-antigen (Li et al., 2003; Wessel et al., 1992). However, there is no need for helicase dimerization during eukaryotic DNA replication, arguing against this model (Yardimci et al., 2010). Alternatively, a single CMG complex motors along dsDNA. As DNA emerges from the rear of CMG's central channel, a proteinaceous pin or "plougshare" bisects the duplex, leading to strand separation (Takahashi et al., 2005). In a variation of this idea, ssDNA exits through side channels midway along the longitudinal axis of MCM (Brewster et al., 2008). In all of these models, DNA enters the MCM central channel as a duplex.

To understand how the replicative helicase interacts with DNA in S phase, we examined the collision of replisomes with various DNA roadblocks in *Xenopus* egg extracts. We previously showed that when two replisomes converge on a DNA interstrand crosslink (ICL), the 3′ ends of the leading strands initially arrest 20-40 nucleotides (nt) from the ICL (Raschle et al., 2008). Here, we provide evidence that the footprint of CMG on DNA underlies these distal arrest points. We had also speculated (Raschle et al., 2008) that the wide distribution of arrest points might suggest that CMG translocates along dsDNA, since the first replisome to arrive at the lesion could engulf the ICL and impose a more distal arrest on the second replisome. However, we show here that blocking the arrival of one replisome using biotin-streptavidin (biotin-SA) roadblocks has no effect on the leading strand arrest points of the other converging replisome. To directly examine the CMG translocation mode, we employed strand-specific roadblocks. We reasoned that if CMG translocates along dsDNA, it should be arrested by a bulky roadblock on either the leading or lagging strand templates. In contrast, if it moves along ssDNA in the 3′ to 5′ direction, it should be arrested by a roadblock on the leading strand template but not on the excluded, lagging strand template. We found that the nascent leading strand stalls ~30 nucleotides from a biotin-SA complex on the leading strand template, consistent with CMG stalling, whereas a biotin-SA complex on the lagging strand template induced little arrest. Similar results were obtained in a single-molecule assay using strand-specific quantum dot (QDot) roadblocks. Together with previous biochemical analyses, our data strongly suggest that CMG unwinds DNA by translocating along ssDNA in the 3′ to 5′ direction, consistent with DNA unwinding by steric exclusion. The data imply a series of discrete molecular events that underlie the conversion of MCM2-7 to an active CMG in S phase.

## RESULTS

To understand how the eukaryotic replicative DNA helicase is configured on DNA in S phase, we examined how the replisome interacts with specific DNA lesions. To this end, we employed nucleus-free *Xenopus* egg extracts (Walter et al., 1998), which support efficient DNA replication of plasmids or λ DNA. In this system, DNA is first incubated with a high speed supernatant of egg cytoplasm (HSS), which chromatinizes the template and also promotes sequence nonspecific MCM2-7 recruitment to the DNA by ORC, Cdc6, and Cdt1 (Arias and Walter, 2004). Subsequently, a concentrated nucleoplasmic extract (NPE) is added, which supports CMG assembly dependent on Cdc7-Drf1, Cdk2-Cyclin E, Mcm10, and Cdc45 (Takahashi and Walter, 2005; Walter and Newport, 2000; Wohlschlegel et al., 2002). The *Xenopus* CMG travels with the replisome and unwinds DNA throughout S phase (Pacek et al., 2006; Pacek and Walter, 2004). These observations indicate that nucleus-free *Xenopus* egg extracts promote activation of the replicative DNA helicase by the same events that occur in cells.

### CMG Binding Correlates with Leading Strand Arrest 20 Nucleotides from a DNA Interstrand Crosslink

We first sought to detect the CMG footprint on DNA in S phase. To this end, we examined the collision of the replisome with two different lesions: a DNA *inter*-strand crosslink, which should arrest CMG, and a DNA *intra*-strand crosslink, which should stall the DNA polymerase but not CMG. Plasmids containing a site-specific cisplatin inter-strand crosslink (pICL$^{Inter}$; Figure 1A, red line) or 1,2 cisplatin intra-strand crosslink (pICL$^{Intra}$; Figure 1B, red bracket) were incubated sequentially in HSS and NPE containing [$\alpha$-$^{32}$P]dATP. At different times after NPE addition, DNA was extracted and digested with StuI, which cuts the plasmid once 268 nt to the right of both lesions (Figure 1A and

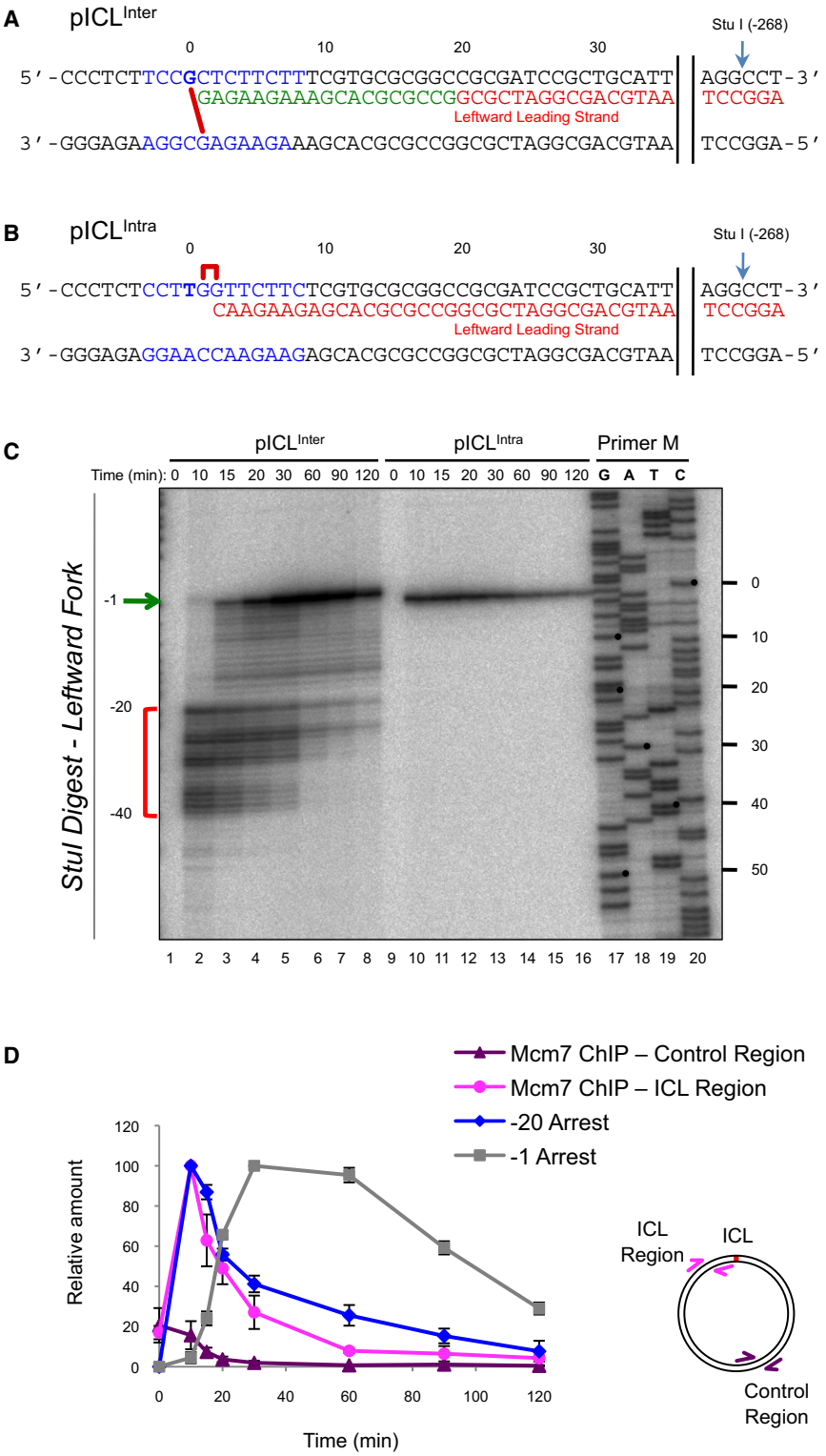


**Figure 1. CMG Causes Leading Strand Stalling ~20 Nucleotides from a DNA Inter-strand Crosslink**

(A) Cartoon depicting the DNA sequence surrounding the ICL in pICL$^{Inter}$. Red line, inter-strand crosslink. Blue arrow, StuI cleavage site, which is used to map leftward leading strands in (C). The sequence of the longest leading strand detected at the 10 min time point (see [C]) is shown in red letters, and the product generated after the leading strand advances toward the ICL after 15 min (see [C]) is shown in green letters. Blue letters, sequence differences between pICL$^{Inter}$ and pICL$^{Intra}$.

(B) Same as (A), except for pICL$^{Intra}$. Red bracket, 1,2 intra-strand crosslink. The sequence of the longest leading strand seen in (C) is shown in red letters.

(C) Mapping leading strands near DNA inter- and intrastrand crosslinks. pICL$^{Inter}$ (lanes 1-8) or pICL$^{Intra}$ (lanes 9–16) was incubated sequentially in HSS and NPE containing [$\alpha$-$^{32}$P]dATP. At the indicated times after NPE addition, replication intermediates were digested with StuI, and separated on a DNA sequencing gel alongside a sequencing ladder generated with primer M (see Figure S1A). The distance of sequencing products from the bold G in panel (A) and T in panel (B) is indicated on the right.

(D) Kinetics of Mcm7 binding to an ICL. pICL$^{Inter}$ was replicated as in (C) but lacking radioactivity, and samples were withdrawn for Mcm7 ChIP using ICL proximal (pink) and control (purple) primer pairs (see plasmid cartoon). The relative ChIP signal adjacent to the ICL (pink circles) and distal to the ICL (purple triangles) was plotted. In parallel reactions containing [$\alpha$-$^{32}$P]dATP, replication intermediates were digested with AflIII, and separated on a DNA sequencing gel alongside a sequencing ladder generated with primer S (see Figure S1A). The leading strands stalled between −20 and −40 and at the −1 position (see Figure S1B) were quantified and plotted (blue diamonds and gray squares). Error bars represent the standard deviation of three experiments.

Figure S1A available online). Leftward leading strands were visualized on a sequencing gel alongside an appropriate sequencing ladder. On pICL$^{Inter}$, the 3′ ends of the leading strands initially stalled 20-40 nucleotides from the ICL (Figure 1C, lane 2, and Figure 1A, red strand)(Raschle et al., 2008). Subsequently, DNA synthesis resumed and the leading strand stalled again 1 nt from the ICL (Figure 1C, green arrow and Figure 1A, green strand) (Raschle et al., 2008). In contrast, during replication of pICL$^{Intra}$, the 3′ end of the leading strand immediately advanced all the way to the lesion, where it stalled (Figure 1C, lanes 10–16; Figure 1B, red strand). These data imply that leading strands arrest 20-40 nt from an *inter*-strand crosslink due to the footprint of the replicative DNA helicase, which we denote as CMG.

To test this idea, we performed chromatin immunoprecipitation (ChIP) for Mcm7, a CMG subunit. pICL$^{Inter}$ was replicated, and at different times, the reaction was crosslinked with formaldehyde, sonicated, immunoprecipitated with Mcm7 antibody, and the recovered DNA amplified with ICL-proximal and control primer pairs (Figure 1D). ChIP revealed that soon after replication began, Mcm7 was depleted from the control region, as expected if CMG travels toward the ICL while displacing any latent MCM2-7 complexes (Figure 1D, purple triangles). In contrast, Mcm7 initially accumulated at the ICL, concurrent with the arrival of leading strands at the −20 position (Figure 1D, compare pink circles and blue diamonds). The subsequent disappearance of Mcm7 from the ICL after 10 min correlated with the disappearance of the −20 to −40 leading strand cluster (Figure 1D), and the advance of the leading strand to the −1 position (Figure 1D, gray squares). These data indicate that arrest of the leading strand 20-40 nt from a cisplatin ICL is caused by the footprint of CMG on DNA (and any dead volume of the DNA polymerase) and that dissociation of CMG facilitates resumption of leading strand synthesis toward the ICL.

## Converging Replisomes Do Not Interfere with Each Other at an ICL

We postulated that the wide range of leading strand arrest points near a DNA inter-strand crosslink (Figure 1C, red bracket) could reflect heterogeneity in the CMG footprint and/or interference by converging CMG complexes. In the latter view, the first CMG to arrive at the ICL would impose a more distal stoppage point on the second replisome, giving rise to the distribution of leading strand products. Such interference might be particularly pronounced if CMG travels along dsDNA, since an ICL might enter deep into the central channel of CMG, allowing the first replisome to prevent approach of the second replisome (Figure S2A, top).

To test whether replisome interference occurs, we designed a plasmid, pICL$^{Lead/Lag}$, in which the arrival of replication forks on one side of an ICL can be blocked. pICL$^{Lead/Lag}$ contains a nitrogen mustard (NM)-like ICL [which causes a −24 position arrest (Raschle et al., 2008)], as well as four biotinylated thymidine nucleotides placed 34-40 nt to the right of the ICL, two on the leading strand template and two on the lagging strand template of the leftward replication fork (Figure 2A). In the presence of SA, the leftward DNA replication fork should not be able to reach the ICL. To test whether this is the case, pICL$^{Lead/Lag}$ was preincubated with and without SA and then replicated in the presence of [$\alpha$−$^{32}$P]dATP. At different times, DNA was digested with StuI and nascent strands of the leftward replication fork were visualized on sequencing gels (Figure 2B). In the absence of SA, the leftward leading strand initially advanced to within 24 nt of the ICL (Figure 2B, lane 1, red bracket), after which it crept forward, nearly reaching the ICL (Figure 2B, lanes 5, 7, 9, 11, 13, green arrow), as expected based on our previous results (Raschle et al., 2008). In the presence of SA, the −24 cluster was largely absent, and we observed a new set of products starting at the −70 position (Figure 2B, lanes 2, 4, 6, 8, 10, 12, orange bracket), which is 30 nt from the outermost biotin-SA complex at the −40 position (Figure 2B, bottom white arrow on DNA sequencing ladder). The arrest of the leading strand 30 nt from the biotin-SA complex is similar to the arrest observed at cisplatin (−20) and NM ICLs (−24). After the leading strand paused for 10-15 min at −70, it was further extended to within one nucleotide of the outermost biotin-SA complex located at the −41 position (Figure 2B, lanes 4, 6, 8, 10, 12, 14, black arrow). We infer that the leading strand arrest at −70 is due to the footprint of CMG, which has stalled at the outermost biotin-SA complex, and that the advance of the leading strand to the −41 position reflects CMG dissociation and advance of DNA polymerase $\varepsilon$ to the lesion. This interpretation is supported by the fact that purified DNA polymerase $\varepsilon$ advanced to within a single nucleotide of a biotin-SA complex in primer extension reactions (Figure S2B). In summary, biotin-SA complexes placed to the right of the ICL efficiently arrest the leftward CMG complex for 10-30 min.

To look for interference of the rightward fork by the leftward fork, pICL$^{Lead/Lag}$ was replicated in the presence and absence of SA and then digested with AflIII, which cuts 151 nt to the left and 581 nt to the right of the ICL (Figure 2A). Strikingly, the −24 arrest pattern of the rightward fork was unchanged by the addition of SA (Figure 2C, blue bracket, compare ± SA lanes), even though the leftward fork was efficiently arrested by the roadblock (Figure S2C, even lanes, orange arrow). We conclude that the presence of a replisome on one side of the ICL does not affect the position of the second replisome on the other side of the lesion. This result can be interpreted in two ways. First, CMG is a dsDNA translocase, but the ICL cannot enter its central channel, preventing the first replisome from engulfing the ICL. However, this explanation is unlikely since the NM-like ICL is nondistorting (A.G., Z. T., S.C., and O.D.S., unpublished data) and does not expand the diameter of the duplex (Angelov et al., 2009). The second interpretation is that MCM2-7 translocates along ssDNA, such that both replisomes arrest just before the ICL, avoiding interference (Figure S2A, bottom).

## Preferential Bypass of a Lagging Strand Roadblock by the Replicative DNA Helicase

To interrogate directly the translocation mode of CMG on DNA, we confronted the replisome with a roadblock on only the leading or lagging strand templates. To this end, we prepared two derivatives of pICL$^{Lead/Lag}$ called pICL$^{Lead}$ and pICL$^{Lag}$, which contain biotins on the leading or lagging strand templates, respectively, for the leftward replication fork (Figures 3B and 3C). Using these DNA templates, we could address how the biotin-SA roadblocks placed on the leading or lagging strand templates influence the leftward moving CMG without interference from the rightward moving CMG, whose arrival is prevented by the ICL (Figure 2C). If CMG translocates along ssDNA in the 3′ to 5′ direction, it will stall at a biotin-SA complex located on the leading strand template, yielding the same −70 leading strand arrest as seen on pICL$^{Lead/Lag}$ (Figures 3A and 3B). In contrast, a biotin-SA complex located on the lagging strand template might not affect CMG progression since this strand would be excluded from the central channel of the helicase (Figure 3C). In this case, the leftward CMG should only stall once it hits the ICL, manifesting as a −24 arrest (Figure 3C). On the other hand, if CMG translocates along dsDNA, it is predicted to stall

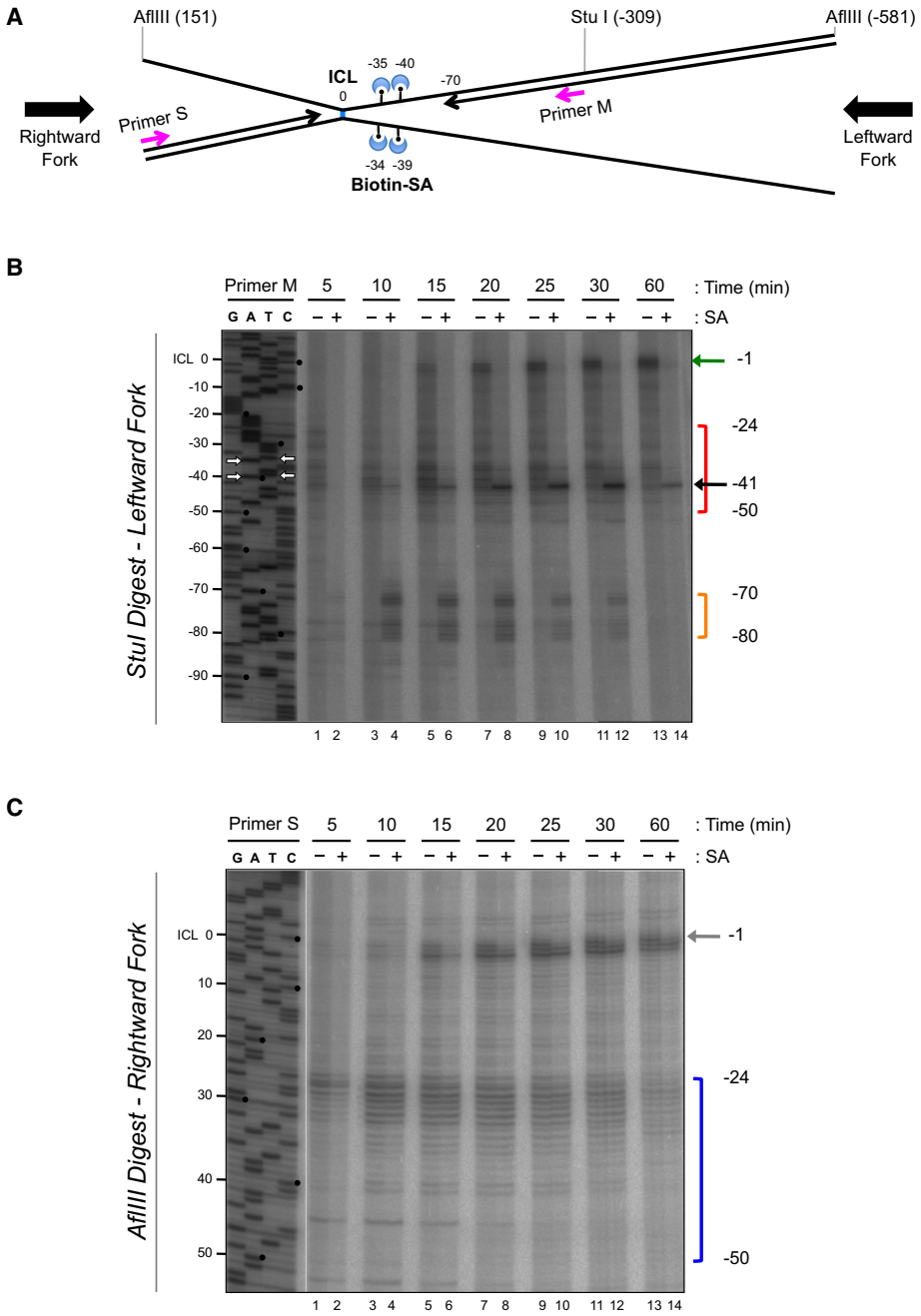


**Figure 2. Replisomes Converging on an ICL Do Not Interfere with Each Other**

(A) Locations of restriction sites, the nitrogen-mustard-like ICL, biotins, and sequencing primers on pICL$^{Lead/Lag}$. Figure S2A presents two alternative scenarios for how replication forks might interact at an ICL.

(B) pICL$^{Lead/Lag}$ was preincubated with buffer or streptavidin, as indicated, and replicated in egg extracts in the presence of [$\alpha$–$^{32}$P]dATP. At the indicated times after NPE addition, replication intermediates were digested with Stu I and separated on a DNA sequencing gel alongside a sequencing ladder generated with primer M. The distance of products from the ICL is indicated on the left of the gel. White arrows on the DNA sequencing ladder indicate the location of biotins. Red bracket, leading strand arrest 24–50 nt from the ICL in the absence of SA. Orange bracket, leading strand arrest 70-80 nt from the ICL in the presence of SA (30–40 nt from the outermost biotin). Green arrow (–1 postion), leading strands that have advanced to the ICL. Black arrow (–41 position), leading strands that have advanced to the outermost biotin-SA complex. Figure S2B shows that DNA polymerase $\varepsilon$ can advance to within one nt of a biotin-SA complex on the leading strand template.

(C) pICL$^{Lead/Lag}$ was preincubated with buffer or streptavidin, as indicated, and replicated in egg extracts in the presence of [$\alpha$–$^{32}$P]dATP. At the indicated times after NPE addition, replication intermediates were digested with AflIII (see Figure 2A) and separated on a DNA sequencing gel alongside a sequencing ladder generated with primer S. Products of the rightward fork are shown. The leftward fork was efficiently arrested by the biotin-SA (see Figure S2C).

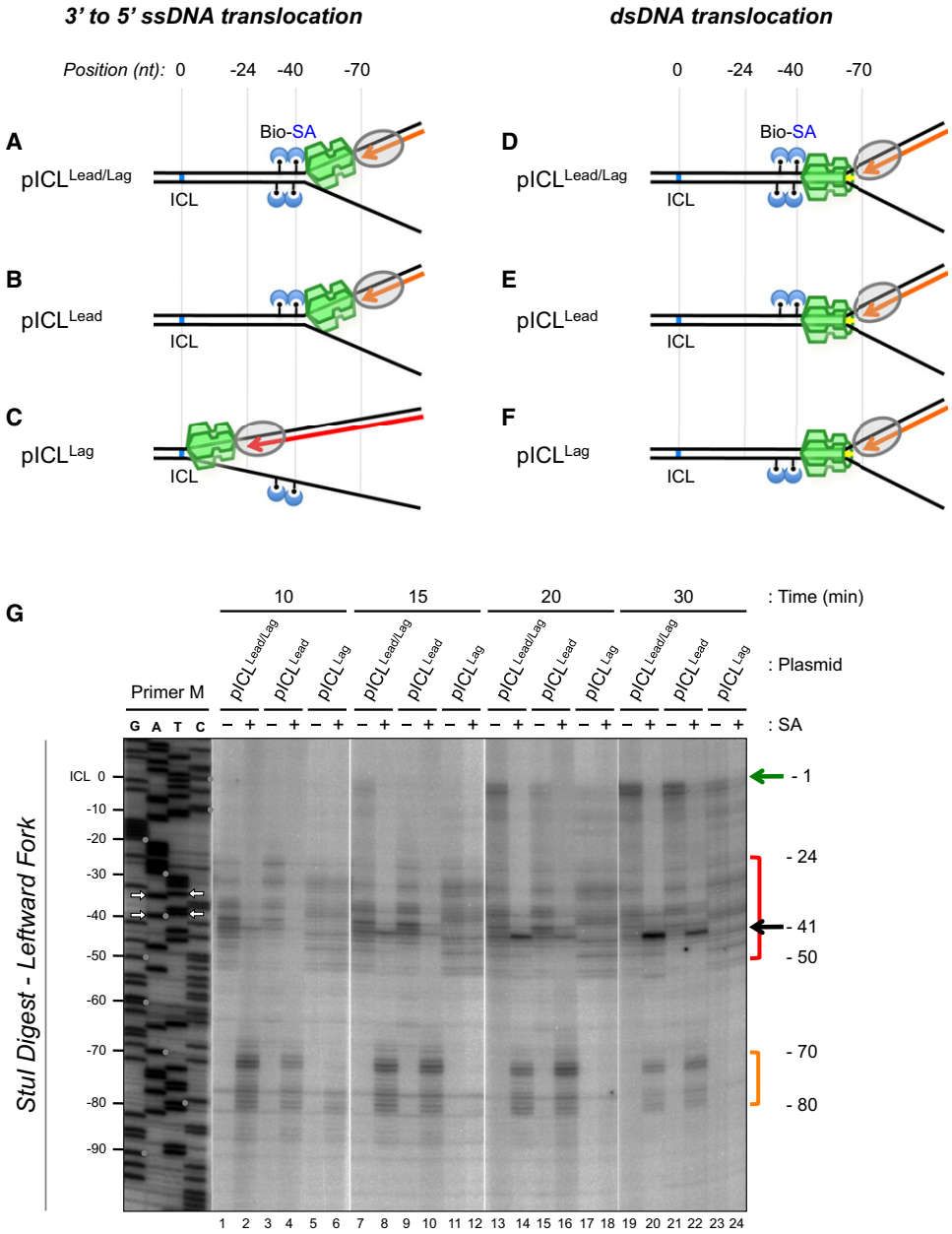


**Figure 3. Biotin-SA Complexes Located on the Leading Strand Template But Not on the Lagging Strand Template Arrest the Replisome**

(A–F) The 3′ to 5′ ssDNA translocation (A–C) and dsDNA translocation models (D–F) for CMG make different predictions regarding how the leftward moving replisome (CMG, green; DNA polymerase, gray) will interact with SA molecules bound to pICL$^{Lead/Lag}$, pICL $^{Lead}$, or pICL$^{Lag}$ (see main text). On all plasmids, the rightward replisome (not depicted) will be prevented from approaching the biotin-SA complexes by the ICL. The yellow line in (D–F) represents the "ploughshare" postulated to split the duplex as it emerges from the central channel. (G) pICL$^{Lead/Lag}$, pICL $^{Lead}$, or pICL$^{Lag}$ was preincubated with buffer or streptavidin, as indicated, and replicated in the presence of [$\alpha$–$^{32}$P]dATP as in Figure 2B. SA was not displaced from pICL$^{Lag}$ during replication (Figure S3).

at the SA whether the obstruction is located on the leading or lagging strand templates since both strands pass through the central channel of the helicase (Figures 3E and 3F; −70 arrest). In short, only if CMG translocates along ssDNA is the leading strand predicted to reach the −24 position on pICL$^{Lag}$ bound to SA (Figure 3C).

pICL$^{Lead/Lag}$, pICL$^{Lead}$, and pICL$^{Lag}$ were replicated separately in the presence or absence of SA, and nascent strands were analyzed after digestion with StuI, as in Figure 2B. When SA was bound to pICL$^{Lead}$, leading strands arrested at the −70 position, almost exactly as seen for pICL$^{Lead/Lag}$ (Figure 3G, compare lanes 2 and 4, 8 and 10, 14 and 16, 20 and 22). In contrast, when

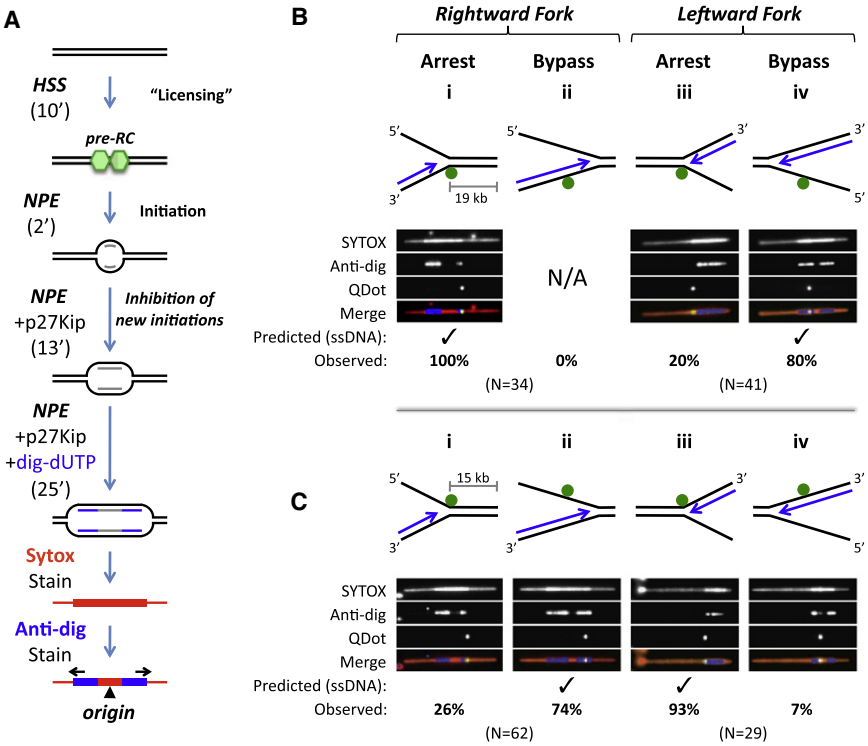


**Figure 4. Single-Molecule Analysis of Replisome Collision with Leading and Lagging Strand-Specific Roadblocks**

(A) Reaction scheme for the replication of immobilized λ DNA in a microfluidic flow cell using a single pair of diverging replisomes. SYTOX Orange and dig-dUTP detection of replicated DNA are indicated schematically. (B and C) λ DNA containing a QDot on the bottom strand (19 kb from the end) or top strand (15 kb from the end), as indicated, was immobilized within a microfluidic flow cell and replicated as depicted in (A). After protein removal, total DNA (SYTOX Orange), dig-dUTP (fluorescein-labeled anti-dig Antibody), and the QDot, were visualized and presented individually or as a merged image. Each dig tract was classified as a rightward or leftward moving fork depending on the location of the origin. If the tract ended within 2 pixels (~0.3 μm) of the QDot, it was considered arrested. Cartoons depicting each type of collision, the expected outcome based on the 3′ to 5′ ssDNA translocation model (checkmarks), representative examples of the raw data, and the frequency of each outcome are included. A hypothetical model in which a dsDNA translocase bypasses a lagging strand roadblock is presented in Figure S4.

biotin-SA was located on the lagging strand template (pICL$^{Lag}$), the result was very different. While a small fraction (maximally 28% of total signal) of leading strands transiently arrested near the −80 position (Figure 3G, lane 6), the majority advanced directly to the −24 position (Figure 3G, lanes 6, 12, 18, and 24, red bracket). Therefore, CMG bypasses a lagging strand roadblock much more readily than a leading strand roadblock.

Using gel shift analysis, we verified that pICL$^{Lead}$ and pICL$^{Lag}$ bound equally to SA (Figure S3A). To assess the retention of biotin-SA complexes on DNA after replication in egg extracts, we immunoprecipitated SA and quantified the associated plasmid by real-time PCR. Importantly, pICL$^{Lag}$ was recovered at least as efficiently as pICL$^{Lead}$, indicating that the absence of replisome arrest at the −70 position on pICL$^{Lag}$ was not due to reduced binding by SA to this DNA template in extracts (Figure S3B). To rule out that SA dissociated from biotin and then reassociated, we added excess free biotin to the replication extract to trap dissociated SA. This manipulation had no significant effect on the retention of SA on either template (compare Figure S3B and Figure S3C; Figure S3D), arguing there was no transient dissociation of the roadblock. The arrest of the CMG by a leading strand but not a lagging strand-specific roadblock clearly favors the 3′ to 5′ ssDNA translocation model.

## Single-Molecule Analysis of Replisome Collisions with Strand-Specific Roadblocks

To examine the interaction of replisomes with strand-specific DNA roadblocks by an independent approach where replisomes do not converge, we employed single-molecule analysis. λ DNA (48.5 kb) biotinylated at one or both 3′ ends was attached to the streptavidinated surface of a microfluidic flow cell. We recently showed that these substrates are extensively replicated by HSS/NPE in an MCM2-7 dependent manner (Yardimci et al., 2010). DNA replication can be limited to a single pair of diverging replisomes when replication initiation is restricted by adding the Cdk2 inhibitor p27$^{Kip}$ shortly after NPE addition (Figure 4A)(Yardimci et al., 2010). Replicated DNA is detected using SYTOX Orange ("SYTOX"), a nonspecific DNA dye, which gives rise to a fluorescence signal that is twice as strong in regions containing two daughter duplexes as in regions containing a single parental duplex (Figure 4A; red molecule). We also added dig-dUTP for the last 25 min of the reaction and then stained the DNA with fluorescent anti-dig antibody (Figure 4A, blue tracts). This allowed us to determine the approximate position of the replication origin, which is located roughly halfway between the stained dig-dUTP tracts, as well as the directionality of each replication fork (Figure 4A) (Yardimci et al., 2010).

For the present study, we attached a quantum dot (QDot; ~20 nm diameter) to the "bottom" strand of λ DNA (see Materials and Methods), 19 kb from the end (Figure 4B$_i$; green dot). Since DNA replication initiates randomly on DNA in *Xenopus* egg extracts, forks hit the QDot from both directions. The QDot resides on the leading strand template for rightward moving replication forks (Figure 4B$_i$ and 4B$_{ii}$) and on the lagging strand template for leftward moving forks (Figures 4B$_{iii}$ and 4B$_{iv}$). If CMG translocates on ssDNA, as indicated by the biotin-SA experiments presented above, leftward forks should bypass the QDot (Figure 4B$_{iv}$), whereas rightward forks should be arrested (Figure 4B$_i$). In contrast, if CMG is a dsDNA translocase,

neither rightward nor leftward forks should be able to bypass the QDot (Figures 4B$_{i}$ and 4B$_{iii}$).

In agreement with the 3′ to 5′ ssDNA translocation model, we found that all rightward DNA replication forks stalled at the QDot (Figure 4B$_{i}$), whereas 80% of leftward forks bypassed the QDot (Figure 4B$_{iv}$). We also attached the QDot to the "top" strand, 15 kb from the end of λ DNA (Figure 4C$_{i}$, green dot). On this DNA template, all polarities are reversed. Thus, if CMG is a 3′ to 5′ ssDNA translocase, leftward forks should stall at the QDot (Figure 4C$_{iii}$) and rightward forks should bypass it (Figure 4C$_{ii}$). In agreement with this prediction, 93% of leftward forks stalled at the QDot (Figure 4C$_{iii}$), whereas 74% of rightward forks bypassed it (Figure 4C$_{ii}$). The fact that 20%–25% of forks stalled at a QDot on the lagging strand template suggests that while CMG is a 3′ to 5′ ssDNA translocase, it can be transiently arrested by a lesion on the excluded strand (see Discussion).

## DISCUSSION

This study addresses whether the eukaryotic replicative DNA helicase (CMG) travels along ssDNA or dsDNA in S phase, a fundamental, unanswered question in cell biology. Our strategy was based on the supposition that both 3′ to 5′ ssDNA and dsDNA translocases should arrest at an obstruction on the leading strand template (Figures 3B and 3E), whereas only a 3′ to 5′ ssDNA should be able to bypass a roadblock on the lagging strand template (Figure 3C versus Figure 3F). Using the arrest point of the leading strand as a marker for CMG stalling, we observed that the helicase was arrested much more efficiently by a leading strand biotin-SA roadblock than a lagging strand roadblock. Analogous results were obtained using single-molecule assays, in which replisomes were collided with QDots. These data support the idea that CMG translocates along ssDNA in the 3′ to 5′ direction. We cannot formally rule out an alternative interpretation of the data in which MCM2-7 translocates along dsDNA and transient opening of the helicase central channel allows bypass of a lagging strand roadblock. However, this model is improbable, principally because it does not explain how the breached helicase could bypass the lesion (see Figure S4 and legend thereof).

Importantly, other aspects of our data are also consistent with CMG being a ssDNA translocase. First, we observed no interference between converging replisomes at an ICL, as might have been expected in the dsDNA translocation model (see Results). Second, the apparent size of the CMG footprint is consistent with a ssDNA translocation model. Thus, upon initial collision of the replisome with a cisplatin ICL, the 3′ end of the leading strand can advance to within 20 nucleotides of the lesion. Given that the longitudinal axis of the eukaryotic MCM2-7 complex comprises ~115 Å (Remus et al., 2009), MCM2-7 should protect ~34 basepairs of dsDNA (115 Å ÷ 3.4 Å per basepair = 34 basepairs), which likely occurs in the context of prereplication complexes. Importantly, ssDNA can be extended to 1.7 times the length of B-form DNA (Smith et al., 1996; van Oijen, 2007). Therefore, 20 nt (34 ÷ 1.7) of fully extended ssDNA would suffice to traverse the entire MCM2-7 channel. Thus, a ssDNA translocation model is compatible with the −20 nt arrest point seen for the leading strand if the active site of DNA polymerase is located immediately behind the rear exit channel of CMG. Although stretching ssDNA to this extent is energetically unfavorable, this might occur as a result of interactions between DNA and the CMG central channel and/or the pulling force exerted by DNA polymerase. It is also worth noting that most of the leading strands arrest further than 20 nt from the ICL, indicating that only a small fraction of stalled CMG complexes encircle fully extended ssDNA. The reason why leading strands arrest 4 nucleotides further away from a nitrogen-mustard like ICL versus a cisplatin ICL (Raschle et al., 2008) is likely that the former lesion stabilizes the duplex, preventing full approach to the lesion by CMG. In the case of SA roadblocks, a steric clash between CMG and SA might explain the more distal arrest point (−30 nt) observed for this lesion.

Finally, our conclusion that the replicative helicase moves along ssDNA is supported by extensive biochemical analysis of purified MCM complexes. Archaeal MCMs (Kelman et al., 1999; Shechter et al., 2000), Mcm4/6/7 (Ishimi, 1997), and CMG (Moyer et al., 2006) exhibit 3′ to 5′ ssDNA translocation activity on model DNA templates. In light of our findings, the observation that MCM complexes can slide (Evrin et al., 2009; Remus et al., 2009) or actively translocate along dsDNA (Kaplan et al., 2003) could have other implications. As previously proposed (Remus et al., 2009), the collision of a replisome with latent MCM2-7 complexes could induce the latter to slide or translocate along dsDNA ahead of the fork. These mobilized MCMs might represent a cadre of reserve helicases that are deployed to rescue stalled replication forks (Remus et al., 2009), or they might serve to increase the local concentration of pre-RCs in unreplicated DNA to potentiate an increased initiation frequency late in S phase (Lucas et al., 2000).

In summary, the data are most consistent with CMG translocation along ssDNA in the 3′ to 5′ direction. The evidence thus indicates that CMG unwinds DNA via steric exclusion, and it strongly disfavors models in which dsDNA passes through any part of the CMG central channel. Future experiments will be required to address the precise molecular mechanism by which CMG translocates along ssDNA and how this leads to strand separation.

### Implications for CMG and Replisome Architecture

Our results have implications for the overall architecture of the DNA replication fork. As discussed above, the −20 nt leading strand arrest point matches precisely what is expected if ssDNA is fully extended within the central channel of MCM2-7. Barring rapid dissociation of replication proteins upon collision with the ICL or a major difference in the dimensions of yeast and *Xenopus* MCM2-7, this observation implies that the C-terminal ATPase domains of the MCM2-7 complex comprise the leading edge of the replisome and that Cdc45, GINS, and any other helicase-associated factors do not substantially alter the footprint of MCM2-7 on DNA. Moreover, the data imply that the active site of DNA polymerase epsilon resides immediately behind the rear exit channel of CMG, which is consistent with our finding that purified pol ε can advance to within 1 nucleotide of a biotin-SA complex on the leading strand template. This configuration is advantageous, as emerging ssDNA will be immediately replicated, minimizing the possibility of strand reannealing or cleavage.

We noted that when a biotin-SA complex was placed on the lagging strand template, there was a low level of transient stalling (Figure 3G, lane 6). Similarly, in single-molecule analysis, QDots placed on the lagging strand template induced ~20% stalling. These results suggest that the excluded strand might interact intimately with the outer face of the CMG, leading to steric clashes with the bulky lesions that cause occasional or transient arrest. Recent structural analysis of the *Drosophila* CMG complex supports this conclusion since it reveals a potential groove/channel on the outer surface of CMG that might interact with the excluded strand (Costa et al., 2011).

## Interactions of the Replisome with DNA Damage

Our data have implications for the early steps of DNA interstrand crosslink repair, which is initiated by the collision of two DNA replication forks with an ICL in *Xenopus* egg extracts (Knipscheer et al., 2009; Raschle et al., 2008). It was previously unknown why leading strands pause at the −20 to −40 positions and then undergo further elongation toward the ICL, followed by lesion bypass. Our experiments indicate that the delay involves the dissociation of CMG from the site of the lesion. Another implication is that when the replisome first arrives at an ICL, the DNA immediately adjacent to the lesion is single stranded since one strand is sequestered within the CMG central channel while the other strand is excluded.

## Implications for the Mechanism of CMG Assembly

In G1, latent MCM2-7 double hexamers appear to interact with dsDNA, as evidenced by the absence of ssDNA within pre-RCs (our unpublished results; Bowers et al., 2004; Geraghty et al., 2000) and the ability of latent MCM2-7 complexes to slide along DNA (Evrin et al., 2009; Remus et al., 2009). Our data indicate that in S phase, CMG encircles ssDNA with no duplex DNA remaining inside the central channel of the helicase. Furthermore, CMG likely functions as a monomer (Gambus et al., 2006; Ilves et al., 2010; Moyer et al., 2006; Yardimci et al., 2010). Assuming these starting and end points, a number of discrete stages can be envisioned that convert MCM2-7 to CMG, not necessarily in the following order (Figure 5). (1) The MCM2-7 double hexamer is split. (2) The latent MCM2-7 rings straddling dsDNA are opened, perhaps via regulation of the Mcm2-Mcm5 gate (Bochman and Schwacha, 2008). Both events might depend on MCM2-7 phosphorylation by DDK. (3) One strand of the DNA duplex is extruded from the central channel, perhaps by the binding of Mcm10 or Sld2 to ssDNA (Kanter and Kaplan, 2010; Warren et al., 2008). (4) The gate is reclosed and the helicase motor is jump-started by Cdc45 and GINS (Ilves et al., 2010). Whatever the precise sequence of events, the reconfiguration of the MCM2-7 complex from a dsDNA binding mode in G1 to a ssDNA binding mode in S phase helps explain why so many initiation factors are required to assemble CMG. This view of initiation establishes a roadmap for future investigations into the functions of replication initiation factors. Notably, the DNA tumor virus initiator proteins E1 and possibly Large T Antigen initially bind to dsDNA within the viral origin of replication but unwind DNA via steric exclusion (Enemark and Joshua-Tor, 2006). Thus, the transition from dsDNA to ssDNA binding appears to be widely conserved among eukaryotic replicative DNA helicases.

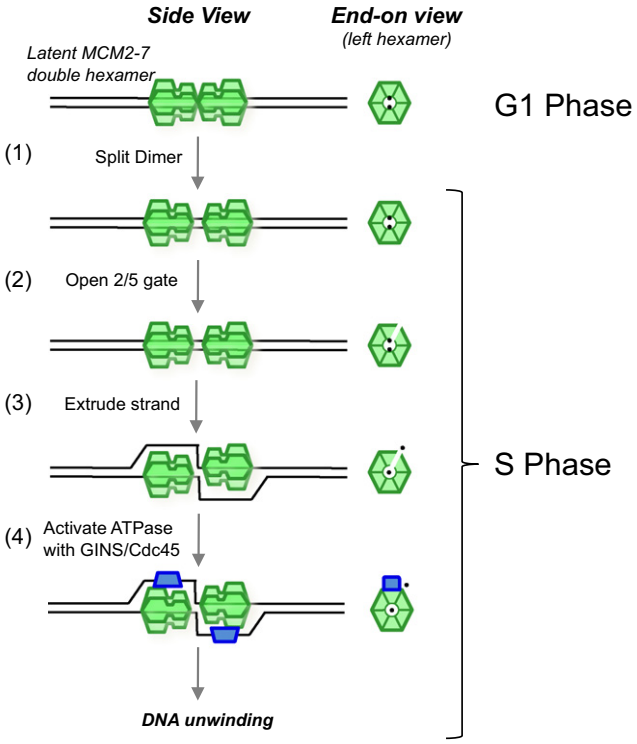


**Figure 5. Model for Replication Initiation**

Model for helicase activation in which MCM2-7 encircles dsDNA in G1 and ssDNA in S phase. See text for details.

## EXPERIMENTAL PROCEDURES

### Preparation of Plasmids

To make pICL$^{Lead/Lag}$, pICL$^{Lead}$, and pICL$^{Lag}$, various ICL-biotin oligonucleotides (see Supplementary Methods) were purified by polyacrylamide gel electrophoresis, and ligated into pSVRLuc to form the three plasmids (see Figure 3) (Guainazzi et al., 2010; Raschle et al., 2008). pICL$^{Control}$ contains the identical sequence as pICL$^{Lead/Lag}$, except for the four biotinylated thymidine nucleotides. pICL$^{Inter}$ and pICL$^{Intra}$ were constructed as previously described (Raschle et al., 2008; Tremeau-Bravard et al., 2004). Compared to pICL$^{Inter}$ and pICL$^{Intra}$, the plasmids pICL$^{Control}$, pICL$^{Lead/Lag}$, pICL$^{Lead}$, and pICL$^{Lag}$ contain a 41 nt insert near the ICL.

### *Xenopus* Egg Extracts and Replication

The preparation of *Xenopus* egg extracts (NPE and HSS) was as described (Walter et al., 1998). For DNA replication, the plasmids (75ng/μl) were first incubated with an equal volume of Streptavidin (5 μg/μl) (SouthernBiotech, Birmingham, AL, USA) or buffer for 1 hr at room temperature (RT), after which this mixture was added to HSS for 5 min at 22°C (12–15 ng/μl final plasmid concentration), followed by addition of two volumes of NPE containing [α−$^{32}$P]dATP. Replication was stopped with Stop Solution (0.5% SDS, 25mM EDTA, 50 mM Tris, [pH 7.5]) at different time points. The purification of DNA replication products was as described (Raschle et al., 2008).

### Nascent Strand Analysis

The nascent strand analysis was carried out as described (Raschle et al., 2008). Briefly, purified DNA replication products were isolated and digested with the indicated enzymes. Restriction fragments were separated on 5% or 7% polyacrylamide sequencing gels. Gels were transferred to filter paper, dried, and nascent strands visualized with a phosphorimager. Sequencing ladders using primers S and M (see Figure 2A) were generated using the

Cycle Sequencing kit from USB (USB Corporation, Cleveland, OH, USA). Quantification was performed by Image Gauge V4.22 (Fuji Photo Film Corporation, Tokyo, Japan).

### Chromatin Immunoprecipitation

Chromatin immunoprecipitation (ChIP) was modified from our existing procedure (Pacek et al., 2006). After the addition of NPE, aliquots of the reaction were crosslinked through the addition of 1% formaldehyde in ELB. After 10 min incubation at RT, glycine was added to stop the crosslinking reaction. The crosslinked material was spun through Micro Bio-Spin 6 Chromatography Columns (BIO-RAD, Hercules, CA, USA) to remove formaldehyde. The flow-through was diluted with sonication buffer and subjected to sonication. Immunoprecipitation with the indicated antibodies and quantitative real-time PCR were performed as described (Pacek et al., 2006). Anti-Mcm7 antibody was previously described (Walter and Newport, 2000); anti-Streptavidin antibody was purchased from Spring Bioscience (Spring Bioscience, Pleasanton, CA, USA).

### Single-Molecule Assays

A QDot was attached to the top strand 15 kb from the right end of λ DNA or to the bottom strand 19 kb away from the end of λ DNA through modification of a previous procedure (Kochaniak et al., 2009; Kuhn and Frank-Kamenetskii, 2008). Anti-digoxigenin antibody (Roche Applied Sciences, Indianapolis, IN, USA) was attached to QDot605 using Invitrogen QDot Antibody Conjugation Kit. After immobilizing λ DNA in the flow cell, 1 nM of anti-digoxigenin conjugated QDot was injected. After 10-20 min incubation, the flow cell was washed with buffer and extracts were introduced. Replication of surface immobilized λ DNA from single initiations in *Xenopus* egg extracts and visualization of replicated products was performed as described (Yardimci et al., 2010). SYTOX, fluorescein labeled anti-dig, and the QDot were imaged using 568 nm, 488 nm, and 405 nm laser light, respectively. To assess replication fork arrest near QDots, replication forks were labeled with dig-dUTP for 25 min. Since the average fork rate in these experiments was 268 bp/minute (Yardimci et al., 2010), uninterrupted replication would yield average dig-dUTP tracts of 6.7 kb (25 min × 0.268 kb/minute). Therefore, only dig-dUTP tracts that were significantly shorter than expected ($\leq$4.5 kb), which ended at a QDot, were considered to represent stalled forks.

## SUPPLEMENTAL INFORMATION

Supplemental Information contains Extended Experimental Procedures and four figures and can be found with this article online at doi:10.1016/j.cell.2011.07.045.

## ACKNOWLEDGMENTS

We thank Milica Enoiu for the gift of pICL$^{Intra}$, Anna Loveland, Puck Knipscheer, and Tatsuro Takahashi for helpful discussions, and the members of our laboratory for valuable feedback on the manuscript. J.C.W was supported by National Institutes of Health (NIH) grant GM62267, by a Leukemia and Lymphoma Scholar Award, and by the American Cancer Society grant RSG-08-234-01-GMC. Y.V.F. was supported by a Human Frontier Science Program Long-Term Fellowship (LT000307/2009). D.T.L was supported by a postdoctoral fellowship (PF-10-146-01-DMC) from the American Cancer Society. O.D.S. was supported by grants from the New York State Office of Science and Technology and Academic Research NYSTAR (C040069) and the NIH (GM08454 and CA092584). A.M.v.O. acknowledges support from the American Cancer Society grant RSG-08-234-01 and Searle Scholarship 05-L-104. J.H. was supported by NIH grant GM034559 and American Cancer Society grant RSG-08-234-01-GMC.

Received: December 15, 2010
Revised: May 17, 2011
Accepted: July 29, 2011
Published: September 15, 2011

## REFERENCES

Angelov, T., Guainazzi, A., and Scharer, O.D. (2009). Generation of DNA interstrand cross-links by post-synthetic reductive amination. Org. Lett. *11*, 661–664.

Arias, E.E., and Walter, J.C. (2004). Initiation of DNA replication in Xenopus egg extracts. Front. Biosci. *9*, 3029–3045.

Arias, E.E., and Walter, J.C. (2007). Strength in numbers: preventing rereplication via multiple mechanisms in eukaryotic cells. Genes Dev. *21*, 497–518.

Bochman, M.L., and Schwacha, A. (2008). The Mcm2-7 complex has in vitro helicase activity. Mol. Cell *31*, 287–293.

Bochman, M.L., and Schwacha, A. (2009). The Mcm complex: unwinding the mechanism of a replicative helicase. Microbiol. Mol. Biol. Rev. *73*, 652–683.

Bowers, J.L., Randell, J.C., Chen, S., and Bell, S.P. (2004). ATP hydrolysis by ORC catalyzes reiterative Mcm2-7 assembly at a defined origin of replication. Mol. Cell *16*, 967–978.

Brewster, A.S., Wang, G., Yu, X., Greenleaf, W.B., Carazo, J.M., Tjajadia, M., Klein, M.G., and Chen, X.S. (2008). Crystal structure of a near-full-length archaeal MCM: functional insights for an AAA+ hexameric helicase. Proc. Natl. Acad. Sci. USA *105*, 20191–20196.

Costa, A., Ilves, I., Tamberg, N., Petojevic, T., Nogales, E., Botchan, M.R., and Berger, J.M. (2011). The structural basis for MCM2-7 helicase activation by GINS and Cdc45. Nat. Struct. Mol. Biol. *18*, 471–477.

Enemark, E.J., and Joshua-Tor, L. (2006). Mechanism of DNA translocation in a replicative hexameric helicase. Nature *442*, 270–275.

Evrin, C., Clarke, P., Zech, J., Lurz, R., Sun, J., Uhle, S., Li, H., Stillman, B., and Speck, C. (2009). A double-hexameric MCM2-7 complex is loaded onto origin DNA during licensing of eukaryotic DNA replication. Proc. Natl. Acad. Sci. USA *106*, 20240–20245.

Fletcher, R.J., Bishop, B.E., Leon, R.P., Sclafani, R.A., Ogata, C.M., and Chen, X.S. (2003). The structure and function of MCM from archaeal M. Thermoautotrophicum. Nat. Struct. Biol. *10*, 160–167.

Gambus, A., Jones, R.C., Sanchez-Diaz, A., Kanemaki, M., van Deursen, F., Edmondson, R.D., and Labib, K. (2006). GINS maintains association of Cdc45 with MCM in replisome progression complexes at eukaryotic DNA replication forks. Nat. Cell Biol. *8*, 358–366.

Gambus, A., Khoudoli, G.A., Jones, R.C., and Blow, J.J. (2011). MCM2-7 form double hexamers at licensed origins in Xenopus egg extract. J. Biol. Chem. *286*, 11855–11864.

Geraghty, D.S., Ding, M., Heintz, N.H., and Pederson, D.S. (2000). Premature structural changes at replication origins in a yeast minichromosome maintenance (MCM) mutant. J. Biol. Chem. *275*, 18011–18021.

Guainazzi, A., Campbell, A.J., Angelov, T., Simmerling, C., and Scharer, O.D. (2010). Synthesis and molecular modeling of a nitrogen mustard DNA interstrand crosslink. Chemistry (Easton) *16*, 12100–12103.

Ilves, I., Petojevic, T., Pesavento, J.J., and Botchan, M.R. (2010). Activation of the MCM2-7 helicase by association with Cdc45 and GINS proteins. Mol. Cell *37*, 247–258.

Ishimi, Y. (1997). A DNA helicase activity is associated with an MCM4, −6, and −7 protein complex. J. Biol. Chem. *272*, 24508–24513.

Kanter, D.M., and Kaplan, D.L. (2010). Sld2 binds to origin single-stranded DNA and stimulates DNA annealing. Nucleic Acids Res. *39*, 2580–2592.

Kaplan, D.L., Davey, M.J., and O'Donnell, M. (2003). Mcm4,6,7 uses a "pump in ring" mechanism to unwind DNA by steric exclusion and actively translocate along a duplex. J. Biol. Chem. *278*, 49171–49182.

Kelman, Z., Lee, J.K., and Hurwitz, J. (1999). The single minichromosome maintenance protein of Methanobacterium thermoautotrophicum DeltaH contains DNA helicase activity. Proc. Natl. Acad. Sci. USA *96*, 14783–14788.

Knipscheer, P., Raschle, M., Smogorzewska, A., Enoiu, M., Ho, T.V., Scharer, O.D., Elledge, S.J., and Walter, J.C. (2009). The Fanconi anemia pathway promotes replication-dependent DNA interstrand cross-link repair. Science *326*, 1698–1701.

Kochaniak, A.B., Habuchi, S., Loparo, J.J., Chang, D.J., Cimprich, K.A., Walter, J.C., and van Oijen, A.M. (2009). Proliferating cell nuclear antigen uses two distinct modes to move along DNA. J. Biol. Chem. *284*, 17700–17710.

Kuhn, H., and Frank-Kamenetskii, M.D. (2008). Labeling of unique sequences in double-stranded DNA at sites of vicinal nicks generated by nicking endonucleases. Nucleic Acids Res. *36*, e40.

Labib, K. (2010). How do Cdc7 and cyclin-dependent kinases trigger the initiation of chromosome replication in eukaryotic cells? Genes Dev. *24*, 1208–1219.

Laskey, R.A., and Madine, M.A. (2003). A rotary pumping model for helicase function of MCM proteins at a distance from replication forks. EMBO Rep. *4*, 26–30.

Li, D., Zhao, R., Lilyestrom, W., Gai, D., Zhang, R., DeCaprio, J.A., Fanning, E., Jochimiak, A., Szakonyi, G., and Chen, X.S. (2003). Structure of the replicative helicase of the oncoprotein SV40 large tumour antigen. Nature *423*, 512–518.

Lucas, I., Chevrier-Miller, M., Sogo, J.M., and Hyrien, O. (2000). Mechanisms ensuring rapid and complete DNA replication despite random initiation in Xenopus early embryos. J. Mol. Biol. *296*, 769–786.

Mendez, J., and Stillman, B. (2003). Perpetuating the double helix: molecular machines at eukaryotic DNA replication origins. Bioessays *25*, 1158–1167.

Moyer, S.E., Lewis, P.W., and Botchan, M.R. (2006). Isolation of the Cdc45/Mcm2-7/GINS (CMG) complex, a candidate for the eukaryotic DNA replication fork helicase. Proc. Natl. Acad. Sci. USA *103*, 10236–10241.

Pacek, M., Tutter, A.V., Kubota, Y., Takisawa, H., and Walter, J.C. (2006). Localization of MCM2-7, Cdc45, and GINS to the site of DNA unwinding during eukaryotic DNA replication. Mol. Cell *21*, 581–587.

Pacek, M., and Walter, J.C. (2004). A requirement for MCM7 and Cdc45 in chromosome unwinding during eukaryotic DNA replication. EMBO J. *23*, 3667–3676.

Pape, T., Meka, H., Chen, S., Vicentini, G., van Heel, M., and Onesti, S. (2003). Hexameric ring structure of the full-length archaeal MCM protein complex. EMBO Rep. *4*, 1079–1083.

Randell, J.C., Fan, A., Chan, C., Francis, L.I., Heller, R.C., Galani, K., and Bell, S.P. (2010). Mec1 Is One of Multiple Kinases that Prime the Mcm2-7 Helicase for Phosphorylation by Cdc7. Mol. Cell *40*, 353–363.

Raschle, M., Knipscheer, P., Enoiu, M., Angelov, T., Sun, J., Griffith, J.D., Ellenberger, T.E., Scharer, O.D., and Walter, J.C. (2008). Mechanism of replication-coupled DNA interstrand crosslink repair. Cell *134*, 969–980.

Remus, D., Beuron, F., Tolun, G., Griffith, J.D., Morris, E.P., and Diffley, J.F. (2009). Concerted loading of Mcm2-7 double hexamers around DNA during DNA replication origin licensing. Cell *139*, 719–730.

Shechter, D.F., Ying, C.Y., and Gautier, J. (2000). The intrinsic DNA helicase activity of Methanobacterium thermoautotrophicum delta H minichromosome maintenance protein. J. Biol. Chem. *275*, 15049–15059.

Smith, S.B., Cui, Y., and Bustamante, C. (1996). Overstretching B-DNA: the elastic response of individual double-stranded and single-stranded DNA molecules. Science *271*, 795–799.

Takahashi, T.S., and Walter, J.C. (2005). Cdc7-Drf1 is a developmentally regulated protein kinase required for the initiation of vertebrate DNA replication. Genes Dev. *19*, 2295–2300.

Takahashi, T.S., Wigley, D.B., and Walter, J.C. (2005). Pumps, paradoxes and ploughshares: mechanism of the MCM2-7 DNA helicase. Trends Biochem. Sci. *30*, 437–444.

Tremeau-Bravard, A., Riedl, T., Egly, J.M., and Dahmus, M.E. (2004). Fate of RNA polymerase II stalled at a cisplatin lesion. J. Biol. Chem. *279*, 7751–7759.

Tye, B.K. (1999). MCM proteins in DNA replication. Annu. Rev. Biochem. *68*, 649–686.

van Oijen, A.M. (2007). Honey, I shrunk the DNA: DNA length as a probe for nucleic-acid enzyme activity. Biopolymers *85*, 144–153.

Walter, J., and Newport, J. (2000). Initiation of eukaryotic DNA replication: origin unwinding and sequential chromatin association of Cdc45, RPA, and DNA polymerase alpha. Mol. Cell *5*, 617–627.

Walter, J., Sun, L., and Newport, J. (1998). Regulated chromosomal DNA replication in the absence of a nucleus. Mol. Cell *1*, 519–529.

Warren, E.M., Vaithiyalingam, S., Haworth, J., Greer, B., Bielinsky, A.K., Chazin, W.J., and Eichman, B.F. (2008). Structural basis for DNA binding by replication initiator Mcm10. Structure *16*, 1892–1901.

Wessel, R., Schweizer, J., and Stahl, H. (1992). Simian virus 40 T-antigen DNA helicase is a hexamer which forms a binary complex during bidirectional unwinding from the viral origin of DNA replication. J. Virol. *66*, 804–815.

Wohlschlegel, J.A., Dhar, S.K., Prokhorova, T.A., Dutta, A., and Walter, J.C. (2002). Xenopus Mcm10 binds to origins of DNA replication after Mcm2-7 and stimulates origin binding of Cdc45. Mol. Cell *9*, 233–240.

Yardimci, H., Loveland, A.B., Habuchi, S., van Oijen, A.M., and Walter, J.C. (2010). Uncoupling of sister replisomes during eukaryotic DNA replication. Mol. Cell *40*, 834–840.